Acta Crystallographica Section A
Foundations of Crystallography
ISSN 0108-7673

Received 15 June 2004
Accepted 12 October 2004

Structures, phase transitions and orientational properties of the C_{60} monomer and polymers

Roger Moret

Laboratoire de Physique des Solides, UMR CNRS 8502, Université Paris-Sud, 91405 Orsay CEDEX, France. Correspondence e-mail: moret@lps.u-psud.fr

The high symmetry and round shape of the fullerene molecules induce orientational phenomena that play an important role in the properties of the fullerene compounds. This is illustrated in this review which is focused on the orientational properties of C_{60} monomer and polymer structures. First, the orientational state of C_{60} at room temperature, its peculiar orientational ordering phase transition and the associated glassy state are described, together with the corresponding temperature–pressure phase diagram. Then, a summary of the polymerization processes and of the varied structures obtained under high-pressure high-temperature conditions or *via* doping by alkali metals is proposed. Finally, some information is given on the orientational properties of C_{60} layers and surfaces.

1. Introduction

The pioneering work of identification of the fullerene molecules (Kroto *et al.*, 1985) followed by their production in large quantities (Krätschmer *et al.*, 1990) has opened up a very exciting field of research which has broadened considerably with the discovery of carbon nanotubes and nanostructures.

The unique properties of the fullerene compounds and derivatives proceed, in particular, from the distinct structure and shape of the fullerene molecules. These all-carbon molecules exhibit closed round shapes where the C-atom bonding is basically sp^2 (as in planar graphite) with some admixture of sp^3 bonding (case of diamond) due to the curvature. They can form molecular solids where the molecules are held together by relatively weak van der Waals forces or accommodate atoms or ions to form a variety of new compounds. The symmetry and ball shape of the fullerene molecules generate orientational degrees of freedom which often play a leading role in the structural and physical properties of these compounds.

Numerous excellent reviews either general (such as the comprehensive book by Dresselhaus *et al.*, 1996) or specialized have dealt with the properties of the fullerenes and of their compounds. Among the most recent topical reviews, we cite those of Rosseinsky (1998) on the chemistry and physics of the metal fullerides, Forró & Mihály (2001) on electronic properties of doped fullerenes, Gunnarsson (1997) on electron correlations and superconductivity, Kuzmany *et al.* (1994) on optical properties, Pintschovius (1996) on neutron scattering and phonons, and Sundqvist (1999) on high-pressure properties.

In the present overview, I have chosen to focus on the structural properties of C_{60} in its monomer and polymer forms. This is motivated by the fact that these topics are representative of the orientational phenomena induced by the fullerene molecules. First, it is clear that the solid-state orientational ordering in monomeric C_{60} provides the basic reasoning for the analysis of the orientational properties of all fullerenes and fullerene compounds. Furthermore, the C_{60} polymers offer a rich set of unusual structures where orientational ordering occurs in one, two and three dimensions.

This article is organized as follows. §2 describes the structural properties and phase transitions of the C_{60} monomer as a function of temperature and pressure. Some emphasis is given to the results obtained from the analysis of the X-ray diffuse scattering intensity distribution and its use as a test of the theoretical intermolecular potentials. In §3, the orientational aspects of polymerization are summarized concerning, in particular, (i) the polymers formed under high pressure and high temperature (§3.2) and (ii) the doped polymers obtained spontaneously by mixing C_{60} with alkali metals (§3.3). Some comments on the importance of C_{60} molecular orientation in films and surfaces are presented in the last section.

2. Structures and phase transitions in crystalline C_{60} (monomer)

In the C_{60} molecule, the 60 equivalent C atoms are located at the vertices of a truncated icosahedron composed of 12 isolated pentagons and 20 hexagons (Fig. 1). The symmetry of the molecule is that of the icosahedral point group I_h with 6 fivefold axes (through the pentagons), 10 threefold axes (through the hexagons) and 15 twofold axes (through the bonds shared by two hexagons). C_{60} can be approximated as a sphere with a diameter of 7.09 Å (neglecting the electronic cloud). Each C atom is bonded to three other C atoms *via* two single bonds and one double bond. The 60 single bonds

forming the pentagonal edges (1.46 Å) are longer than the 30 double bonds shared by two hexagons (1.40 Å) (the C_{60} truncated icosahedron is thus not strictly regular).

2.1. Room-temperature phase

At room temperature, the C_{60} molecules spin about their centers with an average rotational period of about 10 ps. Because of this rapid rotation, except for experimental techniques that have a time resolution in this range, the C_{60} molecules have often been approximated as homogeneous spheres of electron density. Within this model, the molecules form a close-packed face-centered cubic (f.c.c.) average structure with space group $Fm\bar{3}m$ (Heiney *et al.*, 1991). There are four equivalent molecules in the unit cell, located at the special positions (0,0,0), (1/2,1/2,0), (1/2,0,1/2) and (0,1/2,1/2). The cubic lattice parameter is 14.17 Å, the nearest-neighbor C_{60}–C_{60} distance is 10.02 Å and the volume per molecule is 711 Å^3.

Actually, the homogeneous spherical-shell model is an approximation and numerous experimental and theoretical efforts have been made to obtain a more accurate description of the structure and, subsequently, to get a better knowledge of the microscopic intermolecular interactions. The deviations from the model originate from the combination of the specific structure of the C_{60} molecule, with its icosahedral symmetry, and the cubic crystal field where it is placed. This induces two main effects: (i) the average molecular electron density is not isotropic and there are preferred orientations resulting in anisotropic single-molecule orientational probability distributions; (ii) the near-neighbor molecules are not rotating freely but they experience sizeable correlations. These effects have been analyzed in detail by means of a theoretical framework based on the symmetry-adapted function formalism and applied first to C_{60} by Michel and co-workers (Michel *et al.*, 1992; Copley & Michel, 1993). Simultaneously, several empirical intermolecular potentials have been built using different models based on localized or delocalized Lennard-Jones and Coulomb interaction centers. Moreover, while full *ab initio* calculations (using the local-density approximation, LDA) are not technically feasible, the molecular charge density, determined by LDA, has been used to calculate the Coulomb interactions (Savin *et al.*, 1997). These models correctly predict some but not all of the observed physical properties of solid C_{60} (as reviewed by Launois, Ravy & Moret, 1997*a*,*b*, 1999*b*; Chaplot & Pintschovius, 1999; Savin *et al.*, 1997).

Experimentally, the single-molecule orientational probability density, $f(\omega)$, where ω denotes the set of Euler angles that defines the molecular orientation, can be extracted from the analysis of the Bragg reflection intensities. This has been done by several groups using X-ray and/or neutron data (Chow *et al.*, 1992; David *et al.*, 1993*a*; Papoular *et al.*, 1993; Schiebel *et al.*, 1996). Overall, the results are essentially consistent and show the existence of two preferred molecular orientations, denoted P and H therein (David *et al.*, 1992*a*,*b*). This is demonstrated in Fig. 2, where the single-particle mean-field energy, derived using various diffraction data, is plotted as a function of the angle of rotation of the molecule around a molecular threefold axis parallel to a ⟨111⟩ cubic axis. The preferred orientations P and H are shown in Fig. 3. They are such that: (i) molecular symmetry elements (a threefold axis, three mirror planes containing this axis and the three normal twofold axes) coincide with the corresponding symmetry elements in the cubic lattice; (ii) six double bonds, normal to the above threefold axis, straddle cubic ⟨110⟩ directions; and

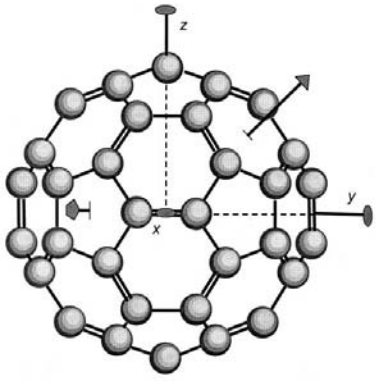

Figure 1
Model of the C_{60} molecule showing the single and double bonds and some of the symmetry elements of the truncated icosahedron. The size of the C atoms has been arbitrarily reduced, for clarity.

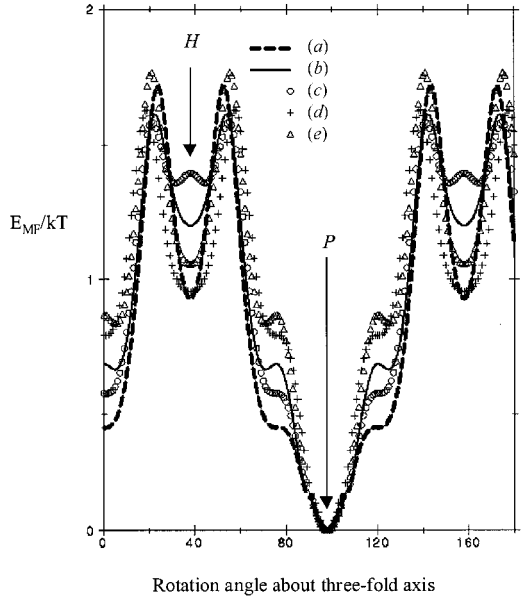

Figure 2
Mean-field energy normalized to the temperature as a function of the rotation angle about a threefold axis (set to 0 for the standard orientation, as in Fig. 1). The energy minimum is arbitrarily set to zero. Different data sets are combined. The calculations are done using the results of Axe *et al.* (1996) for (*a*) $l \leq 12$, (*b*) $l \leq 18$ and of Schiebel *et al.* (1996), $l \leq 18$, (*c*) X-rays, (*d*) neutron, first data set, (*e*) neutron, second data set; l is the index of the icosahedral harmonics used to calculate the molecular form factors. The preferred molecular orientations H (for hexagon, at 38°) and P (for pentagon, at 98°) are described in the text and displayed in Figs. 3 and 4. Reprinted with permission from Launois *et al.* (1999). *Int. J. Mod. Phys.* **13**, 253–281.

(iii) three fivefold axes (normal to pentagons, P case) or three threefold axes (normal to hexagons, H case) lie close to cubic ⟨110⟩ directions.

The experimental orientational probability densities have been compared with those calculated from the various models of intermolecular potential (Launois *et al.*, 1995, 1997). It appears that several potentials, in particular those that involve localized charges, do not agree with the experimental densities. It is found that the models proposed by Lamoen, Michel and Copley with Lennard-Jones interaction centers on the C—C bonds (Lamoen & Michel, 1993; Michel & Copley, 1997) and those proposed by Savin *et al.* (1997) with delocalized molecular charge densities yield the most satisfactory orientational probability densities.

While the Bragg reflections provide information on the average single-molecule orientation, the diffuse scattering intensity and its modulations, distributed in the whole reciprocal space, give information on the nature of the correlations. The diffuse scattering intensity distribution observed in C_{60} powders and single crystals exhibits complex modulations in reciprocal space (Moret *et al.*, 1992, 1993; Copley & Michel, 1993; Launois *et al.*, 1995; Pintschovius *et al.*, 1995). Broad diffuse scattering maxima are located at special points in the Brillouin zone such as *X* (100), *L* ($\frac{1}{2}\frac{1}{2}\frac{1}{2}$) or Γ (000) and elsewhere. Theoretically, the diffuse scattering has been evaluated from the potential models by either a mean-field treatment (Michel & Copley, 1997; Ravy *et al.*, 1996*a*,*b*; Launois *et al.*, 1997*a*,*b*) or molecular-dynamics simulations (Pintschovius *et al.*, 1995; Chaplot *et al.*, 1995). It was found that all potential models account qualitatively for the main diffuse scattering features; quantitatively, however, the models that best reproduced the orientational probability density (Lamoen & Michel, 1994; Michel & Copley, 1997; Savin *et al.*, 1997) also lead to the most satisfactory agreement with the diffuse scattering (Launois, Ravy & Moret, 1997*a*,*b*, 1999).

In principle, the orientational pair correlations could be derived from the diffuse scattering intensity but this analysis would require a large amount of very high precision data. However, some information on these correlations has been gained from molecular-dynamics calculations (using the split-bond charge model, Pintschovius *et al.*, 1995) and from a mean-field calculation, using the potential of Lamoen, Michel and Copley (Lamoen & Michel, 1993; Michel & Copley, 1997). Both studies conclude that near-neighbor C_{60} molecules tend to orientate so that a double bond (DB) on one molecule faces a pentagon or a hexagon on its near-neighbor (so-called P-DB or H-DB configurations), Fig. 4. However, they differ on the importance of some other favorable/unfavorable configurations (configurations characterized by facing hexagons, for instance, are favored by the split-bond charge model while they are excluded by the Lamoen–Michel model). These results are reviewed by Launois, Ravy & Moret (1999) and Chaplot & Pintschovius (1999).

In summary, the structure of the room-temperature phase can be described as follows. On the average, within the $Fm\bar{3}m$ space group, the orientational probability density of a C_{60} molecule fulfills the O_h ($m3m$) point-group symmetry with preferred orientations where double bonds, pentagons and hexagons point towards the ⟨110⟩ directions. The C_{60} molecules perform rapid reorientations (ratcheting motions) between several near-neighbor configurations as a result of competing intermolecular correlations. In particular, C═C double bonds have a marked tendency to face pentagons (P-DB) and hexagons (H-DB) on the neighboring molecule. It is usually considered that these configurations optimize the interactions because electron-rich double bonds on one

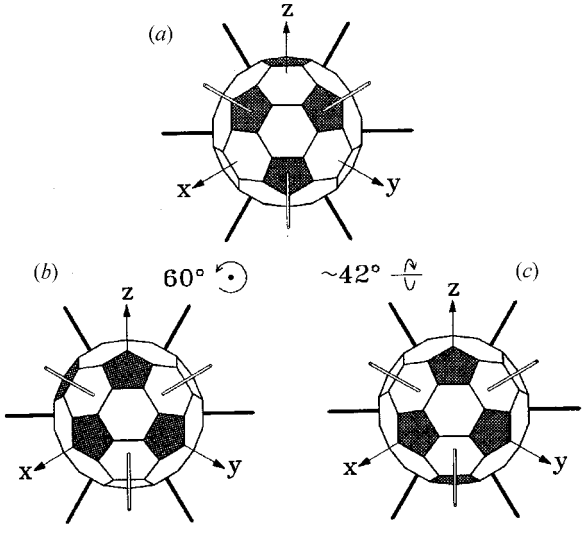

Figure 3
Orientations of a C_{60} molecule with respect to a fixed set of axes. The plane of each drawing is normal to a [111] direction. Thin shaded (unshaded) rods represent ⟨110⟩ directions that are normal (inclined at 35.26°) to the [111] direction. The 12 nearest neighbors of the molecule are in the 12 ⟨110⟩ directions. In (*a*), which represents the majority orientation P, pentagons face neighbors in the 'inclined' ⟨110⟩ directions, and short double (6:6) bonds face neighbors in the 'normal' ⟨110⟩ directions. In (*b*) and (*c*), which represent the minority orientation H, hexagons have replaced pentagons in the 'inclined' ⟨110⟩ directions. The transformation from (*a*) to (*b*) involves 60° rotation about the [111] direction. The transformation from (*a*) to (*c*) involves ~42° rotation about the [1$\bar{1}$0] direction. Reprinted with permission from Copley *et al.* (1994). *Neutron News*, **4**, 20–28

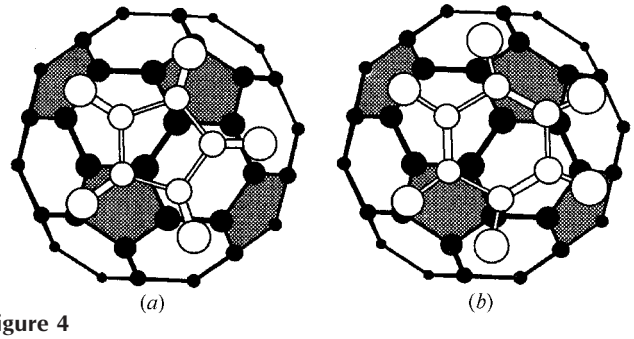

Figure 4
Two views along an axis joining centers of nearest-neighbor C_{60} molecules. In (*a*) a pentagon on the nearer molecule faces a double bond on the more distant molecule; in (*b*) a hexagon faces the double bond on the more distant molecule. Reprinted from Copley *et al.* (1992). *J. Phys. Chem. Solids*, **53**, 1353–1371. Copyright (1992), with permission from Elsevier.

molecule face electron-poor pentagons or hexagons on the neighboring molecules.

2.2. Orientational ordering phase transition – low-temperature phase

As the temperature is decreased, long-range orientational correlations are established, leading to an orientationally ordered structure below $T_o \simeq 260$ K, through a first-order phase transition. The jump and hysteresis displayed by physical quantities such as the thermal expansion clearly establish the first-order character of the transition (Gugenberger *et al.*, 1992). The molecules are orientationally ordered in the low-temperature phase, they are no longer equivalent by translation and each of them has a threefold axis oriented along one of the four ⟨111⟩ axes of the cubic unit cell. This induces a lowering of the symmetry from $Fm\bar{3}m$ to $Pa\bar{3}$ (simple cubic, s.c.).

The molecular orientations are such that near neighbors are in either the P-DB or H-DB configuration described above. The coexistence of these two configurations takes the form of a dynamical orientational disorder where every molecule reorientates rapidly between the two preferred P and H orientations. The average structure has been studied by diffraction experiments as a function of temperature, using for instance high-accuracy Rietveld refinement of neutron diffraction data. The refinements show that the fraction of the more favorable P orientation increases from ~55% just below T_o to 84% at 86 K (David *et al.*, 1992*a*). This is shown in Fig. 5, where the fractional occupancy of the P orientation is well fittted assuming a Boltzmann distribution of P- and H-oriented molecules, except for deviations as T approaches T_o, due to fluctuations. The energy difference between P and H is found to be 11 meV.

Because of the change of Bravais lattice (f.c.c. to s.c.), new reflections appear at the X (100) points of the Brillouin zone.

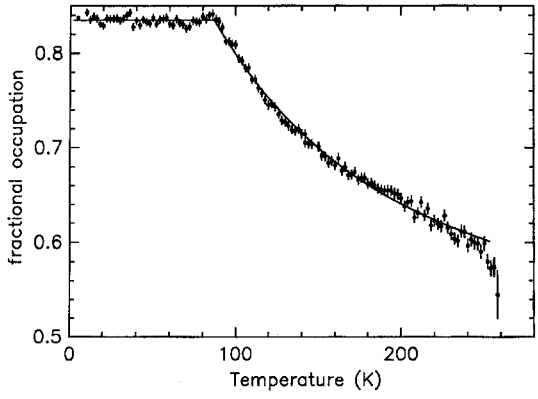

Figure 5
The fractional occupation of the more energetically favorable major orientation as a function of temperature. The quenching of the relative populations of major and minor orientation fractions at the glass transition of *ca* 90 K is clearly evident. The fitted line above 90 K corresponds to a refined energy difference of 122 (4) K [11.0 (3) meV] between the two orientations. There are clear departures from this behavior above 200 K. Reprinted with permission from David *et al.* (1993). *Proc. R. Soc. London Ser. A*, **442**, 129–146.

The temperature dependence of their intensities can be successfully fitted using the same Boltzmann distribution of the P- and H-oriented molecules (with additional small librations, see below) (Moret *et al.*, 1996). These reflections can be analyzed using another approach that considers the condensation of $Fm\bar{3}m$ order parameters of symmetry T_{2g}, T_{1g} and A_{1g} at the X points. The molecular-field equations for these order parameters have been solved (using the Lamoen–Michel–Copley intermolecular potential model) and the temperature evolution of these reflections has also been fitted satisfactorily (Copley & Michel, 1998).

The diffuse scattering due to the disordered P and H molecular orientations has been measured and analyzed to probe the nature of this disorder. Both neutron (Chaplot *et al.*, 1995) and X-ray data (Moret, Launois *et al.*, 1997) confirm that the P/H distribution is random and its temperature dependence, deduced from the neutron data, is in very good agreement with that obtained from the Rietveld refinements. These studies also point to the existence of small librations (2–3°) around the preferred orientations, which is in agreement with the observation of librational modes by inelastic neutron scattering (Neumann *et al.*, 1992; Pintschovius *et al.*, 1995).

The nature of the P/H reorientations has been discussed by David *et al.* (1992*b*, 1993). As seen in Fig. 3, rotations by 60° about ⟨111⟩ or ~42° about ⟨110⟩ transform the P orientation into the H orientation. However, these two reorientations are not equivalent. Rotations about a threefold molecular axis aligned along ⟨111⟩ are uniaxial, involve a large angle of 60° and break all P-DB or H-DB contacts. In the case of rotations about a twofold molecular axis aligned along ⟨110⟩: (i) there is a choice between three equivalent axes such as [110], [101], [01$\bar{1}$]; (ii) the rotation angle is only ~42° and (iii) two of the preferred contacts are preserved during the reorientation (Fig. 3) (David *et al.*, 1993). The latter reorientations are thus more appealing as confirmed by calculations of a smaller rotational hindrance potential for the ⟨110⟩ rotations (Schiebel *et al.*, 1996; Wulf *et al.*, 1999).

2.3. Glass transition – frozen orientational disorder

As shown in Fig. 5, the fraction of P orientation saturates below about 90 K and the reorientations thus appear to be frozen in (David *et al.*, 1992*a*). This glassy state is obtained when the thermal energy is not sufficient to overcome the potential barrier (~250–300 meV) that separates the two orientational configurations. It has been characterized in detail by a number of techniques, notably specific heat (Matsuo *et al.*, 1992) and high-resolution dilatometry measurements (Gugenberger *et al.*, 1992). As the ratcheting motion slows down upon cooling, the observed freezing temperature actually depends on the time scale of the experimental technique that is used (Schranz *et al.*, 1993; Moret, 1993). These effects have been reviewed by Meingast & Gugenberger (1993), who showed that the relaxation times deduced from the different experiments follow an Arhenius dependence over about 15 decades.

2.4. Pressure–temperature phase diagram (monomer)

Because of the strong C—C molecular bonds, pressure has little effect on the shape and size of the C_{60} molecule. On the other hand, the van der Waals intermolecular interactions are strongly pressure sensitive. A number of experimental and theoretical studies have evaluated the C_{60} bulk modulus (Sundqvist, 1999) and the best measured value for the f.c.c. phase at room temperature and ambient pressure is B_0 = 9.6 GPa (Pintschovius *et al.*, 1999). Theoretical values calculated from various empirical potential models are comparable or higher. A relatively good knowledge of the low-temperature–'low'-pressure phase diagram of the C_{60} monomer (Fig. 6) has been built from a variety of experimental results, as reviewed in detail by Sundqvist (1999) and summarized below.

In the orientationally ordered s.c. phase and the glassy state, it is interesting to note that the H orientation occupies a 6% smaller volume than the P orientation (Gugenberger *et al.*, 1992; David *et al.*, 1993). It follows that the fraction of H-oriented molecules increases with pressure (David & Ibberson, 1993) and the bulk modulus of the 'H phase' is found to be about 10% smaller than that of the 'P phase' (Pintschovius *et al.*, 1999).

The orientational ordering transition temperature T_o increases under pressure, as determined by a number of techniques. There is a spread of experimental values for dT_o/dP mainly because some pressure-transmitting gases, such as He, intercalate into C_{60}, which yields an extrinsic pressure dependence. The currently accepted intrinsic value of dT_o/dP is about 165 K GPa^{-1} and at room temperature (299 K) the orientational ordering transition takes place at about 224 MPa (Samara *et al.*, 1993; Lundin & Sundqvist, 1996; Pintschovius *et al.*, 1999).

As the H orientation is favored under pressure, the energy difference between the two orientations vanishes at a weakly temperature dependent pressure of about 0.2 GPa. It corresponds to a 50–50 distribution of H and P orientations (dashed line in Fig. 6). At higher pressure, the fraction of P-oriented molecules decreases and the question of a fully ordered state has been debated. Based on calculations of the intermolecular energy (Burgos *et al.*, 1994), Sundqvist (1999) postulated the existence of a 'lock-in' transition to a completely ordered state that should occur near 10% P, *i.e.* within the shaded region shown in Fig. 6.

The transition temperature to the glassy state also increases with pressure, with a slope dT_g/dP of 62 K GPa^{-1} (dotted line in Fig. 6), as determined, in particular, by measurements of the thermal conductivity (Andersson *et al.*, 1996).

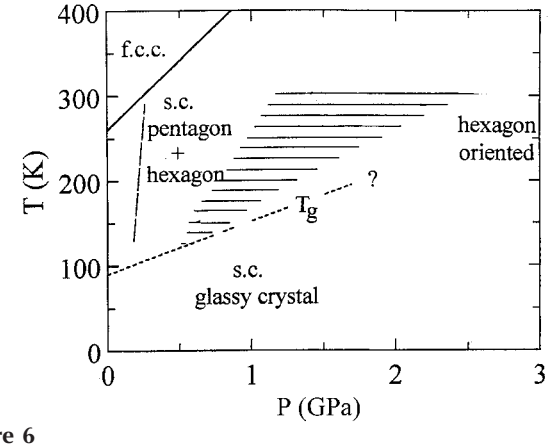

Figure 6
Phase diagram of monomeric C_{60}. The solid line denotes the f.c.c.–s.c. transition and the dotted line the glass transition. The dashed line corresponds to the equilibrium between P- and H-oriented molecules, *i.e.* a 50/50 [P]/[H] distribution. The shaded area indicates the region where a 'transition' to an H-oriented state should occur. Reprinted with permission from Sundqvist (1999). *Adv. Phys.* **48**, 1–134.

3. C_{60} polymerization – orientational aspects

A large family of new compounds and derivatives of C_{60} can be prepared by means of solid-state reactions, fullerene derivative chemistry and electrochemistry. The electrophilic character of C_{60} and the presence of 30 double bonds often determine the corresponding reaction mechanisms. An important class of compounds consists of the so-called C_{60} polymers where one, two or several double bonds open on each C_{60} molecule, allowing various types of intermolecular bonding to form (Fig. 7). These polymerization mechanisms occur under various conditions such as when exposing C_{60} to intense laser light, electrons or plasma discharge, applying high-pressure–high-temperature treatments or transferring electrons to neutral C_{60} as in the alkali-doped compounds. In this section, we describe the structure and formation of these polymers in the light of their orientational properties.

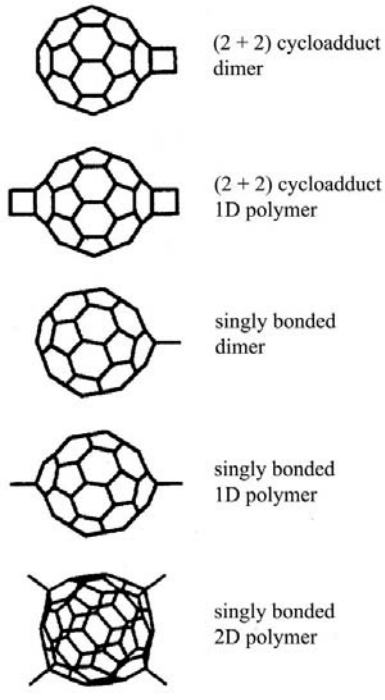

Figure 7
Molecular geometry of various C_{60} dimers and polymers with singly and doubly bonded molecules. Reprinted from Pekker *et al.* (1998). *Science*, **265**, 1077–1078. Copyright (1998), with permission from Elsevier.

3.1. Photopolymerization

Early in the study of fullerenes, it was recognized that C_{60} molecules polymerize when irradiated by intense UV or visible light (Rao *et al.*, 1993). The resulting material is insoluble in toluene and returns to pristine C_{60} if heated above about 400 K. Spectroscopic data give evidence for the formation of two intermolecular single bonds generating four-membered rings between neighboring molecules (so-called 2 + 2 cycloaddition) (Fig. 7). Because of the small penetration depth of the light (0.1–1 μm), this polymerization is only effective in films or at the surface of bulk or powder samples. Furthermore, it only occurs in the room-temperature phase (above 260 K) where the (almost) free rotation of the molecules allows double bonds on adjacent molecules to be parallel thus enabling the formation of four-membered rings.

The structure of the photopolymerized units is still being debated. It was proposed that dimers form primarily above $T \sim 350$ K while larger polymers (short chains, clusters) may be produced below $T \sim 320$ K (Burger *et al.*, 1996). From the analysis of Raman spectroscopic results, Wågberg *et al.* (1999) proposed that a significant number of branched chains are induced by photopolymerization. In any case, it is considered that these polymerized units are highly disordered.

3.2. High-pressure–high-temperature polymers

Polymerization under high-pressure–high-temperature conditions is certainly the most studied procedure and this is motivated, in particular, by the prospect of synthesizing extremely hard three-dimensional polymers. Furthermore, there is a large body of data being used in an attempt to understand the structure and conditions of stability of the various dimer, chain and layer polymers. These results were reviewed by Blank, Buga *et al.* (1998) and Sundqvist (1999). Many questions remain open due to the complexity of the P–T diagram and the fact that most measurements were made *ex situ* after quenching the samples back to normal conditions.

3.2.1. Dimers. By shortening the interfullerene distance, pressure creates favorable conditions for the opening of double bonds and the formation of four-membered rings (2 + 2 cycloaddition) that link a C_{60} molecule with one of its 12 near neighbors along the equivalent ⟨110⟩ directions of the parent f.c.c. lattice (Fig. 8). This mechanism has been shown to occur above about 1 GPa and at, or slightly above, room temperature (Davydov *et al.*, 1999) resulting in the formation of C_{60} dimers, the first stage towards polymerization. Theoretically, various structural arrangements of these dimers have been elaborated and compared using a minimization of the lattice energy and the most stable structures have been identified (Dzyabchenko *et al.*, 1999*a*). In contrast, experimental results indicate that the dimers are disordered in position and orientation within an average cubic lattice derived from that of the monomer (Davydov *et al.*, 1999; Moret, Launois *et al.*, 2004). This is illustrated in Fig. 9 showing the two-dimensional section of a model crystal that was built numerically to fit the X-ray diffuse scattering distribution produced by a crystal primarily formed of dimers. Actually, some weak correlations probably exist and may stabilize trimers (either linear or triangular) and small clusters derived from the structural arrangements proposed by Dzyabchenko *et al.* (1999*a*).

It is interesting to note that, depending on the pressure and the path through the pressure–temperature diagram, the formation of the dimers begins either within the f.c.c. phase where the C_{60} molecules rotate almost freely or within the s.c.

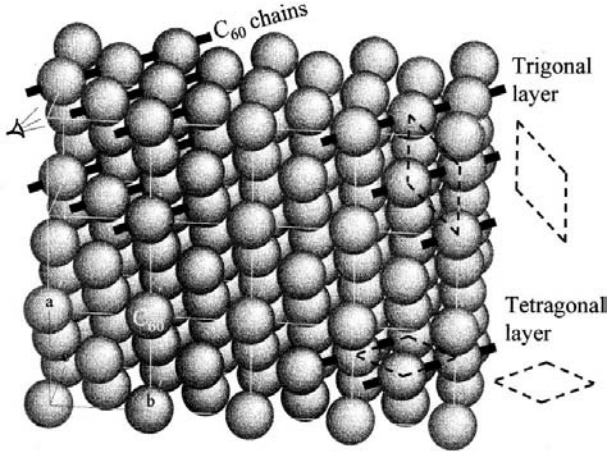

Figure 8
Schematic representation of the relation between the C_{60} monomer, 1D and 2D C_{60} polymer structures. The fullerene molecules are represented by spheres (radius 3.5 Å). The f.c.c. monomer (a, b, c) unit cell is shown at the bottom left. The C_{60} chains (solid black segments) of the orthorhombic polymer are shown at the top left. The formation of the trigonal and tetragonal layers by connection of the chains is sketched on the right. In this sketch, the ~9% contraction of the $C_{60}-C_{60}$ distance due to the formation of the covalent bonds is neglected. Reprinted with permission from Moret *et al.* (2000). *AIP Conf. Proc.* **544**, 81–84.

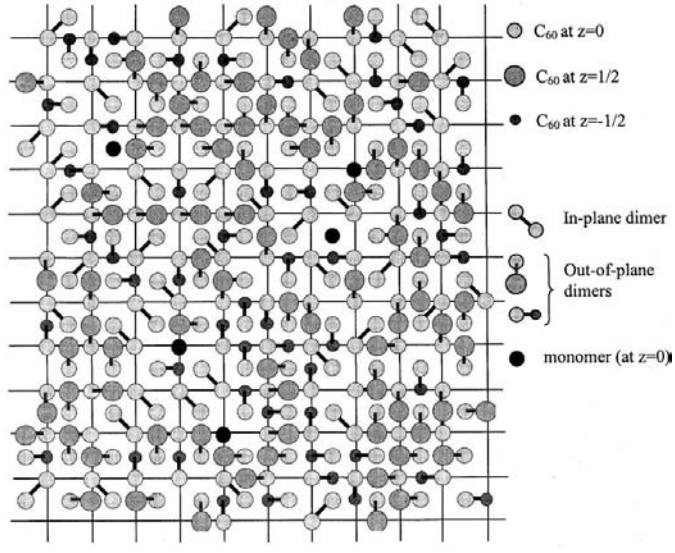

Figure 9
Random distribution of the C_{60} dimers (and isolated monomers) in the (001) plane of a model crystal that accounts reasonably well for the experimental diffuse scattering intensity distribution. Only in-plane and out-of-plane C_{60}'s that form dimers with an in-plane C_{60} are shown. Reprinted with permission from Moret *et al.* (2004). *Eur. Phys. J.* **37**, 25–37.

phase with near neighbors in the P-DB or H-DB configurations (Fig. 6). In fact, the H-DB configuration is stabilized by pressures exceeding about 1 GPa and in this configuration small librations are sufficient to bring the double bonds in parallel orientation, as required for bonding (Marques *et al.*, 1996). In any case, the nature of the parent phase does not appear to influence significantly the disordered dimer organization.

3.2.2. 1D polymers. The next stage of polymerization is obtained for temperatures in the 500–600 K range and it consists in the condensation of two four-membered rings per C_{60} molecule and the formation of chains. While the possibility of disordered branched chains is suggested by some Raman data (Wågberg *et al.*, 1999), most powder and single-crystal diffraction studies have reported the existence of parallel straight chains that form ordered orthorhombic structures. These chains can form along one of the six $\langle 110 \rangle$ directions as illustrated in Fig. 8, which shows how the chains proceed from the monomer structure (in this figure, the C_{60}'s are represented by spheres). Two different structures labelled *O* and *O′* have been observed and it is considered that they correspond to high- (above ~2–3 GPa) and low-pressure ranges, respectively. These structures are characterized by different 'orientations' of the chains around their axes (the 'orientation' is here defined as the angle formed by the chain link constituted by the four-membered ring joining the molecules, as represented in Fig. 10). In the *O* structure (pseudo-tetragonal *Immm* space group), the chain links are parallel to the $(a_o c_o)$ plane (Nuñez-Regueiro *et al.*, 1995) while, in the *O′* structure (orthorhombic *Pmnn* space group), they are alternately tilted by an angle $+\mu$ and $-\mu$ from chain to chain (Fig. 10) (Agafonov *et al.*, 1997; Moret, Launois, Persson & Sundqvist, 1997). The angle μ is difficult to estimate from experiments [for instance 29 and 45° provide similar fits to the diffraction data (Moret, Launois, Persson & Sundqvist, 1997)] but a comparison of the relative stabilities of these two structures, using intermolecular potentials adapted from those described in §2.1, has shown that the *Pmnn* structure is slightly more stable, with $\mu \sim 30°$ (Dzyabchenko *et al.*, 1999*b*,*c*).

3.2.3. 2D polymers. For temperatures and pressures in the ranges 700–900 K and 1.5–9 GPa, one obtains four or six four-membered rings per C_{60} molecule. This leads to 2D polymerization within the $\{100\}_c$ and $\{111\}_c$ layers of the parent cubic monomer structure, respectively. The formation of the polymer layers by cross-linking of the chains is illustrated in Fig. 8, which shows the corresponding tetragonal and trigonal unit cells. These layers are then stacked in a close-packed arrangement to form ordered tetragonal or rhombohedral structures, which are represented schematically in Fig. 10. The cross-linking of the chains by supplementary four-membered rings is indicated by the broken lines and the different

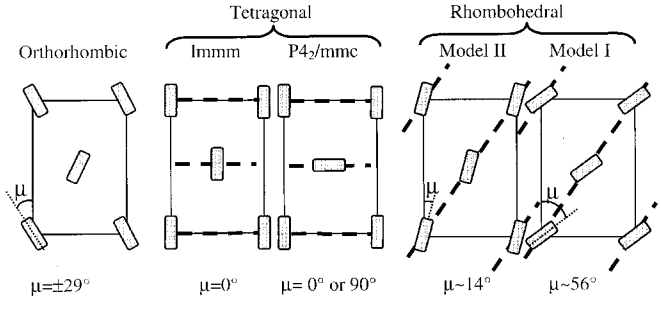

Figure 10
Schematic views of the polymer chains, running along $\langle 110 \rangle_{cubic}$ directions of the parent monomer lattice, for the different polymer structures. The chains are normal to the figure (in Fig. 8, they are viewed along the direction marked by the eye). The 'chain orientation', defined as the orientation of the chain link or four-membered rings, is represented by shaded bars that form an angle μ with the $\langle 001 \rangle_{cubic}$ directions. The broken lines represent the 2D tetragonal and rhombohedral polymer layers that can be obtained, at least schematically, by connecting the C_{60} molecules of the chains by supplementary four-membered rings. Reprinted with permission from Moret *et al.* (2000). *AIP Conf. Proc.* **544**, 81–84.

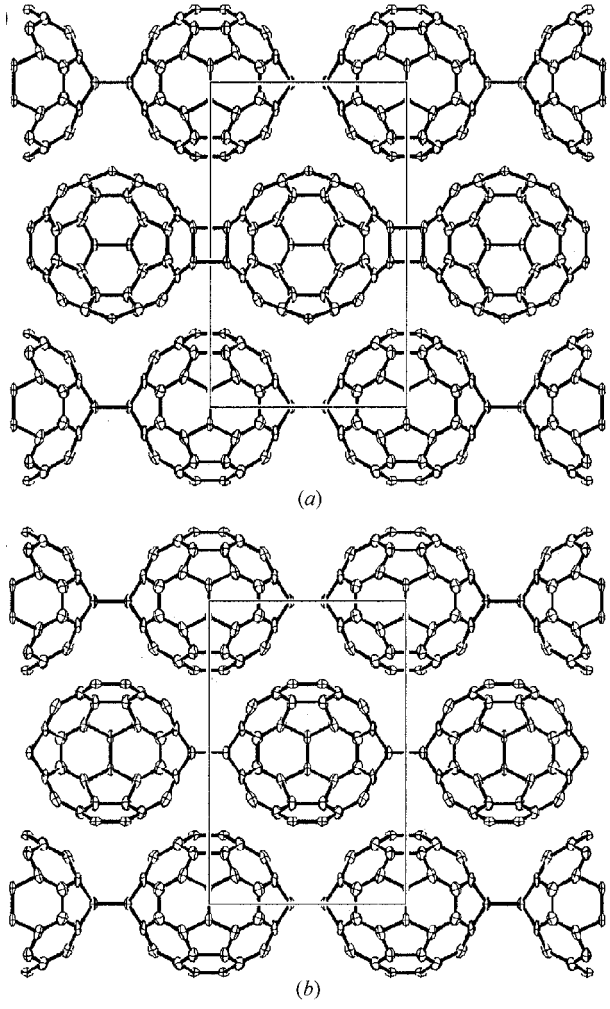

Figure 11
Projections along b_{tet} of the (*a*) $P4_2/mmc$ and (*b*) *Immm* polymer structures. The C_{60} layers, perpendicular to the figure, are stacked along the vertical c_{tet} direction [originating from the *a* (*b* or *c*) direction of the cubic structure of the C_{60} monomer, see Fig. 8]. In (*a*) the four-membered rings are alternately perpendicular and parallel to the plane of the figure while in (*b*) all are perpendicular. Reprinted from Narymbetov *et al.* (2003). *Chem. Phys. Lett.* **367**, 157–162. Copyright (2003), with permission from Elsevier.

stackings discussed below are shown. These structures have been studied in detail both theoretically and experimentally.

If we consider first the tetragonal structure, usually observed below about 4–5 GPa, two types of stacking can be stabilized depending on the temperature–pressure treatment. In the *Immm* orthorhombic structure (actually pseudo-tetragonal because a_{ort} and b_{ort} are almost equal), adjacent layers are just shifted to form a close-packed arrangement of the C_{60} molecules while in the $P4_2/mmc$ case they are additionally rotated by 90° around the stacking axis c_{tet} (4_2 screw axis, originally a cubic *a*, *b* or *c* direction). This is shown in Fig. 11 where the C_{60} layers (horizontal) are projected along b_{tet} and stacked along the vertical c_{tet} direction. For $P4_2/mmc$ (Fig. 11*a*), the four-membered rings are alternately parallel and perpendicular to the figure while for *Immm* (Fig. 11*b*) they are all perpendicular (and project as a single bond). Theoretically, the lattice energy of the $P4_2/mmc$ stacking was calculated to be lower than that of the *Immm* stacking (Dzyabchenko *et al.*, 1999*b*,*c*).

There seems to be an agreement on the fact that the $P4_2/mmc$ structure is favored when the temperature is increased before the pressure is applied ('heating-then-pressing' path) (Moret *et al.*, 2000*a*; Moret, Wågberg & Sundqvist, 2004; Narymbetov *et al.*, 2003). The 'pressing-then-heating' path is more controversial. The *Immm* structure was originally proposed (Nuñez-Regueiro *et al.*, 1995) and confirmed recently on single crystals treated at 2.5 GPa and 773 K (Chen & Yamanaka, 2002). However, using a similar path, a mixture of rhombohedral polymer and disordered dimers was obtained at 2 GPa and 700 K (Moret, Wågberg & Sundqvist, 2004). Note that this pressure is outside the approximate pressure range, 4–9 GPa, of the rhombohedral polymer. Furthermore, Davydov *et al.* (1998) showed that the tetragonal polymer can be obtained from the rhombohedral polymer upon decreasing the pressure from 6 to 2.2 GPa at 873 K.

Two types of structure (both described in the $R\bar{3}m$ space group) have also been considered for the rhombohedral polymer. In type I (Nuñez-Regueiro *et al.*, 1995), the trigonal layers shown in Fig. 12(*a*) are stacked according to the *ABCABC* sequence (where *A*, *B* and *C* denote the positions of C_{60} centers in successive layers). However, an alternative structure (type II) was calculated to be more favorable energetically (Dzyabchenko *et al.*, 1999*b*). This structure corresponds to a rotation of 60° of all molecules relative to the former structure, as shown in Fig. 12(*b*) (preserving the same *ABCABC* stacking). Let us point out that the second structure can be described, equivalently, by a different stacking, *ACBACB*, of the layer shown in Fig. 12(*a*). These structures, although similar, exhibit an important difference as the contacts between the stacked molecules involve pentagons in structure I and hexagons in structure II. Experimental single-crystal X-ray diffraction studies confirmed the existence of structure II (Moret *et al.*, 2000*a*) and refined its atomic structure (Chen *et al.*, 2002). Recent theoretical studies, in the framework of the density-functional theory, found either equal total energy for the two structures (Okada & Oshiyama, 2003) or a slightly lower energy (by 0.01 eV/C_{60} only) for structure II (Miyake & Saito, 2003).

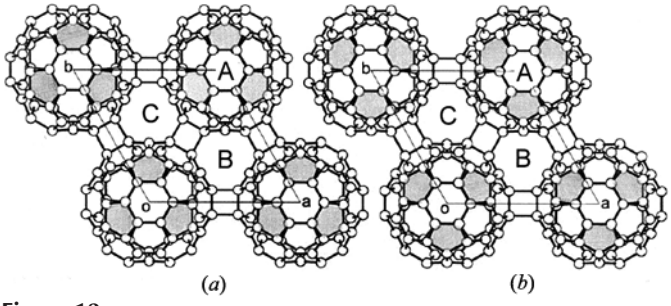

Figure 12
Projection of the C_{60} 2D network of the 3*R* phase along the c_{rhom} stacking direction for the structure proposed by (*a*) Nuñez-Regueiro *et al.* (1995) and (*b*) Dzyabchenko *et al.* (1999*b*). These layers are stacked according to the sequence *ABCABC* where *A*, *B* and *C* denote the positions of C_{60} centers in successive layers. The pentagonal faces are shadowed to clarify the difference between the two arrangements. Note that the *ACBACB* stacking of layer (*b*) is actually equivalent to the *ABCABC* stacking of layer (*a*). Reprinted from Chen *et al.* (2002). *Chem. Phys. Lett.* **356**, 291–297. Copyright (2002), with permission from Elsevier.

Let us note that isotropic polymerization may lead to disordered states because molecules bond in all equivalent near-neighbor directions. This creates frustrated configurations and may prevent long-range-ordered structures to form. By applying a uniaxial stress, Marques *et al.* (2003) have shown that it is possible to select the bonding direction and obtain better ordered structures.

3.2.4. 3D polymers. As noted above, there is a strong interest in 3D polymers because of the possibility of synthesizing extremely hard C_{60} polymers under high pressure, either hydrostatic or non-hydrostatic (Ruoff & Ruoff, 1991). However, in spite of numerous studies (as reviewed by Sundqvist, 1999; Blank, Buga *et al.*, 1998), the situation is somewhat unclear due to experimental difficulties and the problems associated with the combination of *ex situ* studies (hampered by possible uncontrolled changes after treatment) with (relatively few) *in situ* experiments. The general qualitative picture is as follows. For pressures higher than about 8–9 GPa, a cubic (f.c.c.) structure is observed up to about 600–700 K. It is more and more disordered as the temperature is raised and covalent bonds form in all directions (increasing the hardness and bulk modulus close to that of diamond, 443 GPa). For instance, Bennington *et al.* (2000) have reported a disordered f.c.c. (broad diffraction peaks) structure with a short 12.5 Å parameter at 12 GPa. When the pressure exceeds about 9.5 GPa, the existence of body-centered structures has also been reported. The structure becomes amorphous when the temperature is raised further, above 900–1000 K (Blank, Denisov *et al.*, 1998; Brazhkin *et al.*, 1996) because the molecules themselves collapse leading to a disordered network of 3D sp^3 bonds. At higher temperatures, one obtains graphitic structures.

Under non-hydrostatic conditions, various 'superhard' phases have been prepared and studied (using primarily X-ray diffraction and Raman spectroscopy). Apart from amorphous phases, containing cubic diamond crystallites (Hodeau *et al.*, 1994), several studies have reported the existence of relatively

well defined 'superhard' structures. At 13 GPa and 820 K, Marques *et al.* (1999) observed an elliptical deformation of the X-ray Debye–Scherrer rings because of the anisotropic compression and found evidence for 3D polymer structures. Serebryanaya and co-workers (Serebryanaya & Chernozatonskii, 2000; Serebryanaya *et al.*, 2001) used a shear deformation anvil cell and obtained two types of body-centered orthorhombic structures with in-plane 2 + 2 cycloaddition (as in the 2D tetragonal polymers) combined with 3 + 3 interlayer bonding (Fig. 13).

Another approach followed theoretical predictions (using the local-density approximation) of the transformation of the tetragonal structure into a 3D polymer structure (Okada *et al.*, 1999). Léger *et al.* (2002) found no such effect but a progressive amorphization between 10 and 29 GPa. However, strong indication for this transformation to occur around 20 GPa was first given by *in situ* Raman studies at room temperature (Meletov *et al.*, 2001). An *in situ* Raman study of the isothermal (800 K) compression of both tetragonal and rhombohedral phases showed that they transform into 'superhard' phases at about 23 and 12 GPa, respectively (Talyzin & Dubrovinsky, 2003). Furthermore, *in situ* X-ray measurements showed that a first-order irreversible transition occurs around 24 GPa for the tetragonal polymers, inducing a shortening of the *c* axis (Dam Hieu Chi *et al.*, 2003). This is interpreted as the signature of 3D polymerization through deformation of the C_{60} molecules and cross-linking of the tetragonal layers by 3 + 3 cycloaddition, in agreement with Serebryanaya's model. Fig. 13 shows how the C_{60} layers of the tetragonal polymer, formed by 2 + 2 cycloaddition, are connected by bonds such as $C_1 - C_5^*$ and $C_5 - C_1^*$ (where C_1^* and C_5^* denote C atoms from the neighboring layer). The bulk modulus of the resulting 3D network of C_{60} molecules was found to be 407 GPa, *i.e.* only slightly smaller than that of diamond (Dam Hieu Chi *et al.* 2003).

3.2.5. Polymer transformations and pressure–temperature diagram. While our knowledge of the pressure–temperature diagram of the HPHT polymers has largely improved in the last decade, considerable work is still needed because of fundamental and technical reasons. For instance, most *ex situ* experiments produce metastable samples that may evolve during or after quenching to ambient conditions. Treatment times may often be too short (such as 1 min or less at very high pressures) in comparison with the slow kinetics of formation and transformation of the polymer structures. This is revealed at high pressure (12.5 and 14.3 GPa) by the time-resolved experiments of Horikawa *et al.* (2001) indicating that the cell parameter of the f.c.c. lattice diminishes continuously over as much as 3 h. Similarly, at lower pressure and temperature (such as 1.5 GPa, 300–400 K), the formation of the dimers and orthorhombic polymer evolves continuously over a few hours (Davydov *et al.*, 1999).

The influence of the path through the *P–T* diagram (already pointed out in §3.2.3) and the complexity of the polymer transformations are noteworthy. In the heating-then-pressing path, 1D or 2D polymerization proceeds from rapidly rotating monomers (f.c.c. orientationally disordered phase). Although this could lead to disordered states because of the formation of chains in all directions, orientational variants with relatively well ordered orthorhombic or tetragonal structures have been produced. The pressing-then-heating path involves precursor monomers that are H-oriented (§2.4) and 2 + 2 cycloaddition requires small reorientations (§3.2.1). Again, the resulting dimers – considered as an intermediate stage towards the formation of polymer chains or layers – are orientationally disordered. However, the strains associated with the molecular displacements linked to dimerization may lift the orientational degeneracy and promote linear or planar bonding to develop as the temperature is increased. Concerning the 2D polymers, it was suggested that the heating-then-pressing path may indeed favor the formation of triangular trimers in {111} planes (instead of trimers or clusters located in {100} planes), thus leading preferentially to rhombohedral polymers (Talyzin & Dubrovinsky, 2003) in agreement with recent results by Moret, Wågberg & Sundqvist (2004) (see §3.2.3).

The orientational aspects of the 1D–2D polymer transformations can be analyzed by considering the chains as basic units, as shown in Fig. 10 (we recall that the chain orientation is here defined by the orientation of the four-membered rings joining the molecules, as explained in §3.2.2). It reveals that the orthorhombic (*Pmnn*) to tetragonal (for both pseudo-tetragonal *Immm* and $P4_2/mmc$) transformations schemati-

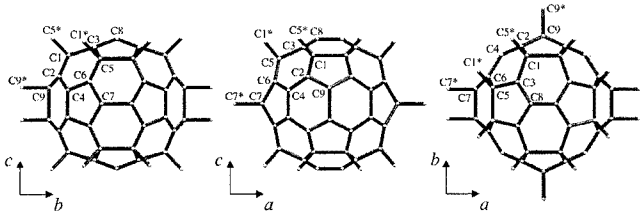

Figure 13
Structural model for the 3D *Immm* structure derived from that of the 2D tetragonal polymer. Note that the molecules are linked by 2 + 2 cycloaddition in the (*ab*) layer while the interlayer bonding involves 3 + 3 cycloaddition. Reprinted with permission from Dam Hieu Chi *et al.* (2003). *Phys. Rev. B*, **68**, 153402-1–4. Copyright (2003) by the American Physical Society.

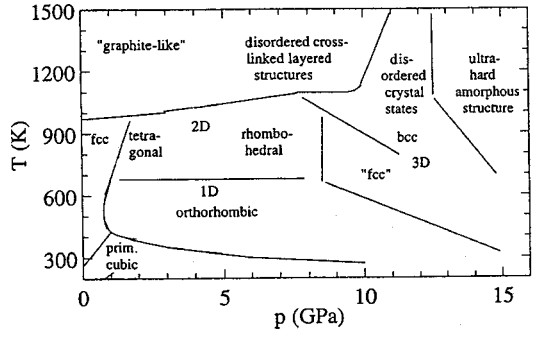

Figure 14
Simplified 'reaction' phase diagram for C_{60} showing the structures observed after short time treatment at the corresponding temperatures and pressures. A more detailed version of this diagram was given by Blank, Buga *et al.* (1998). Reprinted with permission from Sundqvist (2001). *Phys. Status Solidi B*, **223**, 469–477

cally involves proper rotations of the chains followed by interchain cross-linking in $\{100\}_c$ planes. Using the same scenario, the orthorhombic-to-rhombohedral transformations require all chains to rotate in order to possess the same orientation, although the orientation angle μ is different for the *ABC* and *ACB* structures. It is difficult to estimate whether such reorientations of the chains are possible energetically; if so they would represent an attractive mechanism for the formation of the 2D polymers (Moret *et al.*, 2000*b*; Moret, Wågberg & Sundqvist, 2004). On the other hand, the tetragonal–rhombohedral transformation (or *vice versa*) involves different polymer planes and it requires more drastic rearrangements, *i.e.* breaking the layers into small units or even dimers (Wågberg *et al.*, 2005).

To conclude this section, we show in Fig. 14 a simplified tentative pressure–temperature diagram indicating the different structures that have been identified. We emphasize again that in most cases the studies have been performed on metastable products after quenching to ambient conditions. Moreover, some results are contradictory and do not fit in this diagram [such as the stabilization of the tetragonal *Immm* structure up to at least 20 GPa, before 3D polymerization, as mentioned in §3.2.4 (Dam Hieu Chi *et al.*, 2003)].

3.3. Doped polymers

C_{60} can be doped in several ways, by substitution of foreign atoms for C atoms on the ball, by endohedral doping (*i.e.* inside the shell) or by inserting guest atoms between the molecules (exohedral doping). The latter procedure has given rise to an active field of research, focused, in particular, on the properties of the superconducting alkali metal fullerides A_3C_{60} (A = K, Rb, Cs) and of the A_xC_{60} compounds and polymers. In the polymer case, the charge transfer from the alkali metals provides electrons to the molecules which, under adequate conditions, may dimerize or form 1D or 2D polymers. The unusual structural properties of these polymers are reviewed below.

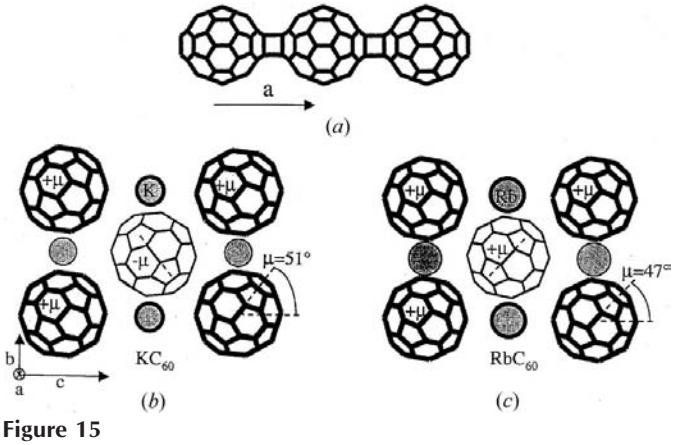

Figure 15
(*a*) Sketch of the polymer chain running along **a** in the AC_{60} polymer structures. Models of the (*b*) KC_{60} and (*c*) RbC_{60}/CsC_{60} structures. In (*b*) and (*c*), heavy (light) lines correspond to in-plane (out-of-plane) molecules and alkali atoms. Note that the orientation μ of the molecules alternates (+μ, −μ) in KC_{60} while it is the same for RbC_{60} (and CsC_{60}). Reprinted with permission from Launois *et al.* (1999). *AIP Conf. Proc.* **486**, 47–51.

3.3.1. AC_{60} polymers. When K, Rb or Cs is mixed in stoechiometric amount with C_{60}, the alkali metal intercalates into the octahedral sites of the f.c.c. structure at about 600–700 K. Upon slow cooling below a first-order structural change at 350–400 K, the C_{60} molecules form ionized 1D chains by 2 + 2 cycloaddition along one of the six equivalent ⟨110⟩ directions, with a short intermolecular distance of ~9.1 Å (Winter & Kuzmany, 1992; Chauvet *et al.*, 1994; Pekker *et al.*, 1994). The resulting compounds are stable in air. They exhibit different electronic properties and ground states that are not clearly understood: KC_{60} is described as a 3D metal with a non-magnetic metal–insulator transition at 50–60 K (Hone *et al.*, 1995) while RbC_{60} and CsC_{60} are considered as quasi-1D systems with a transition near 40–50 K towards an insulating magnetic ground state (as reviewed by Forró & Mihály, 2001). These contrasted properties and ground states are certainly related to subtle differences in the structure of these salts, as explained below.

The AC_{60} polymers form pseudo-body-centered orthorhombic structures similar to those of the 1D high-pressure high-temperature C_{60} polymer (§3.2.2). Stephens *et al.* (1994) determined the KC_{60} and RbC_{60} structures using powder X-ray diffraction but the relative orientations of the chains could not be ascertained (as in §3.2.2, the 'orientation' is defined by the plane of the four-membered ring formed by 2 + 2 cycloaddition). Single-crystal X-ray work (Launois *et al.*, 1998) showed that they are different in the K and Rb salts, as described by the *Pmnn* and *I*2/*m* space groups with $\mu \sim 51$ and 47°, respectively (Fig. 15). This was confirmed by a detailed powder neutron diffraction study, which also revealed significant distortions of the molecules (Huq *et al.*, 2001) while a powder high-resolution X-ray study of CsC_{60} showed that it is isostructural with RbC_{60} with $\mu \sim 46°$ (Rouzière *et al.*, 2000). An essential difference between the *Pmnn* and *I*2/*m* structures is that the chain orientation alternates along *b* and *c* in KC_{60} while it is the same for all chains in RbC_{60} and CsC_{60} (Fig. 15). The relative stability of these structures has been calculated by taking into account the C_{60}–C_{60} and alkali-metal–C_{60} interactions (Verberck, Michel & Nikolaev, 2002; Verberck, Nikolaev & Michel, 2002). The direct intermolecular interactions were found to favor the *Pmnn* structure while the alkali–C_{60} interactions favour *I*2/*m*. In RbC_{60} and CsC_{60}, the second effect (in particular the quadrupolar alkali-mediated interaction) dominates. This is attributed to the larger quadrupolar polarizability of the Rb^+ and Cs^+ ions with respect to K^+ ions (Verberck, Michel & Nikolaev, 2002).

The structure–property relationship of the AC_{60} polymers is further enriched by their low-temperature behaviors. The metal–insulator transition in KC_{60} is accompanied by a structural transition at ~60 K stabilizing a superstructure that manifests itself by weak additional Bragg reflections. This superstructure is defined by (**a** + **c**, **b**, **a** − **c**), where **a**, **b**, **c** refer to the room-temperature orthorhombic unit cell and it doubles the unit-cell volume. Verberck, Nikolaev & Michel (2002) proposed that it is caused by orientational charge-

density waves (modulating the valence-electron density) along the polymer chains associated with displacements of the surrounding K^+ ions and that it is specific of KC_{60}. Fig. 16 displays these structural changes: the molecular charge distributions, represented by contour plots, are tilted by about 13° clockwise and counterclockwise from chain to chain, alternately, along the *a* and *c* directions. Furthermore, the alkali-metal ions are shifted within the (*ac*) plane. The lattice periodicity is unchanged along **b**. This attractive model remains to be evaluated by comparison of the calculated and measured intensities of the superstructure reflections or (better) by low-temperature structure refinement. In the case of RbC_{60}, there is no evidence for any structural change that could be associated with the low-temperature insulating magnetic state. On the other hand, a lattice contraction was found to occur in CsC_{60} below 14 K (Rouzière *et al.*, 2000) and it could be related to the occurrence of the non-magnetic spin-singlet state found by NMR at the same temperature (Simovič *et al.*, 1999).

3.3.2. A_xC_{60} polymers. Apart from the above 1D AC_{60} polymers, several other doped fullerenes can polymerize, with various structures and properties. To begin with, instead of slow cooling, AC_{60} can form dimers upon quenching from above 400 K down to below 270 K (Zhu *et al.*, 1995; Oszlányi *et al.*, 1995). The structure of these charged $(C_{60})_2^{2-}$ dimers is different from that of the high-pressure high-temperature dimers because the C_{60}'s are now linked by single C—C bonds. The corresponding monoclinic structure ($P2_1/a$) is shown in Fig. 17 for RbC_{60} and the atomic positions could be resolved from the Rietveld refinements using the LeBail technique, indicating the absence of orientational disorder for the dimers (Oszlányi *et al.*, 1996). Note that the dimers are slightly tilted away from the *c* axis, in the (*ac*) plane. This dimer structure can be stabilized at low temperature but transforms into the polymeric form upon heating above 270 K, *via* a complex route involving a cubic intermediate stage where the dimers dissociate before reforming four-membered rings (Kosaka *et al.*, 1995; Gránásy *et al.*, 1996).

A similar type of bonding with C—C single bonds is found in the Na_2AC_{60} (*A*: K, Rb, Cs) polymers slowly cooled from the high-temperature f.c.c. phase (Prassides *et al.*, 1997) [for Na_2CsC_{60} an additional moderate pressurization is also needed (Margadonna *et al.*, 1999)]. While the polymerization is complete in Na_2KC_{60}, it is only partial in Na_2RbC_{60} and Na_2CsC_{60}, where the polymer phase was found to be mixed with the superconducting simple cubic phase (Margadonna *et al.*, 1999). However, Schirber *et al.* (2001) claimed to have obtained pure Na_2CsC_{60} polymer and that this compound is also superconducting (but with T_C lower by ~3 K than that of the cubic phase, *i.e.* 11.5 K). In the polymer compounds, the C_{60} molecules form linear chains that are arranged in a monoclinic structure ($P2_1/a$) as shown in Fig. 18 (Bendele *et al.*, 1998). This was deduced by Rietveld refinement of high-resolution X-ray powder diffraction patterns and optimization of the orientation of the C_{60} molecules (as the atomic positions could not be refined independently, owing to the relatively large number of atoms). The preferred orientation indicates that these are connected by single C—C bonds along the *c* axis. Furthermore, the Rietveld refinement is significantly better for single C—C bonds than for 2 + 2 cycloaddition (Bendele *et al.*, 1998).

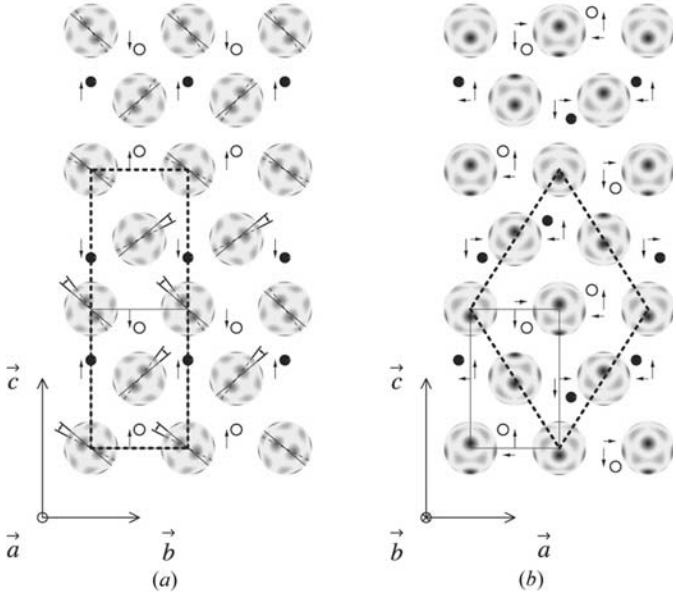

Figure 16
Model for the low-temperature structural modulation in KC_{60}. (*a*) Projection onto the crystallographic (*bc*) plane and (*b*) projection onto the (*ac*) plane. The molecular charge distributions, represented by contour plot projections are rotated ±13° away from their original *Pmnn* structure. This rotation is indicated by the dashed lines in (*a*), rotated clockwise or counter clockwise relative to the original solid lines. The circles represent the alkali-metal ions which are shifted from their original positions as shown by the arrows (exaggerated for clarity), resulting in the (**a + c**, **b**, **a** − **c**) superstructure. In (*a*) and (*b*) the molecules at the origin are at level zero and the alkali-metal ions represented by solid (or empty) circles are at level zero (or 1/2). The radius of the C_{60}^- units has been reduced for clarity. Reprinted with permission from Verberck *et al.* (2002). *Phys. Rev. B*, **66**, 165425-1–14. Copyright (2002) by the American Physical Society.

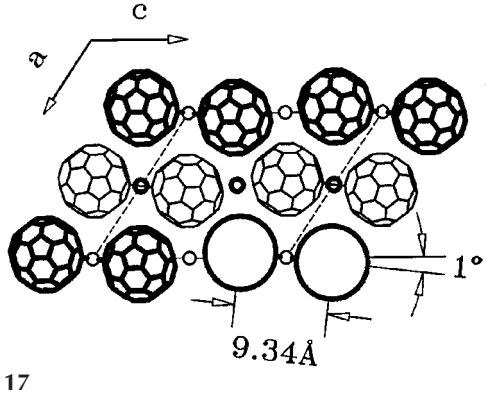

Figure 17
Monoclinic lattice of the dimer phases of AC_{60}. The lower right corner shows the structureless dimer and the rest of the lattice shows the atomic configuration of RbC_{60}. Note the tilt of the dimer axis relative to **c**. Bold and normal fullerenes and alkali atoms are at $y = 0$ and $y = 1/2$, respectively. Reprinted with permission from Oszlányi *et al.* (1996). *Phys. Rev. B*, **54**, 11849–11852. Copyright (1996) by the American Physical Society.

The factors that determine the type of bonding, 2 + 2 cycloaddition or single C—C bonds, in the various dimers and polymers, have been clarified following theoretical and experimental studies (Bendele *et al.*, 1998; Pekker *et al.*, 1998). It was found that the charge state of the fullerene is a key parameter. Neutral fullerenes (as in the high-pressure high-temperature dimers and polymers) or singly charged fullerenes (as in the 1D AC_{60} compounds) are linked *via* 2 + 2 cycloaddition. Covalent bonding *via* single C—C bonds requires 2 electrons per bond and this is favored when more charges are introduced by doping. It explains that the $(C_{60})_2^{2-}$ dimers in AC_{60} and the C_{60}^{3-} chains in Na_2AC_{60} are formed *via* single bonds.

This is also in agreement with the occurrence of the same type of bonding for C_{60}^{4-} ions in the 2D Na_4C_{60} polymers. This 2D polymerization occurs under prolonged heating of C_{60} and Na at normal pressure (Oszlányi *et al.*, 1998). The C_{60} molecules are linked to four neighbors by single C—C bonds and form polymer layers in the $(10\bar{1})$ plane, as outlined by heavy lines in Fig. 19. There is a twofold orientational disorder of the C_{60} molecules by rotation around the *b* axis in the monoclinic structure (space group *I*2/*m*). The C_{60} layers are interleaved by the Na atoms located in distorted tetrahedra. Actually, there are two different types of tetrahedra so that the corresponding Na^+ sites are not equivalent. Li_4C_{60} is another interesting 2D doped polymer (Yasukawa & Yamanaka, 2001; Tomaselli *et al.*, 2001) that, in contrast, was reported to have double C═C bonds (Yasukawa & Yamanaka, 2001). This was recently confirmed by Wågberg *et al.* (2004) by Raman spectroscopy and X-ray diffraction and the authors proposed a tetragonal structure very similar to that of the undoped C_{60} 2D polymers (the X-ray data did not allow the *Immm* and $P4_2/mmc$ structures to be distinguished, see §3.2.3). The difference in structure between Li_4C_{60} and Na_4C_{60} can be explained either by the smaller Li size or a weaker charge transfer from Li to C_{60} (Wågberg *et al.*, 2004).

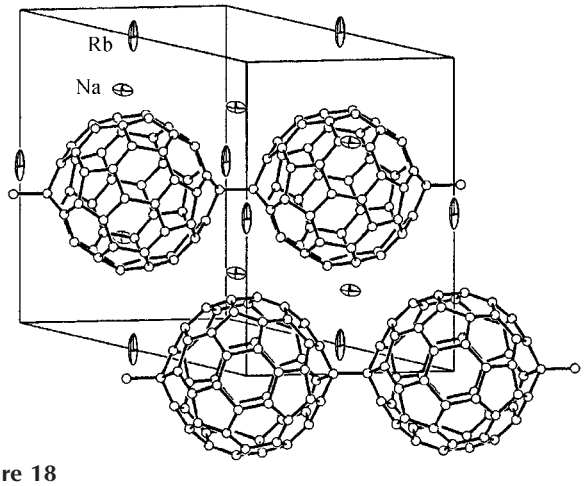

Figure 18
Crystal structure of the Na_2RbC_{60} polymer. The unit cell is monoclinic (space group $P2_1/a$) with parameters a = 13.711, b = 14.554, c = 9.373 Å, β = 133.53° (at 180 K) and derives from the cubic room-temperature structure by a 0.6 Å contraction along one of the cubic face diagonals and a 0.4° tilt of one of the axes. Reprinted with permission from Bendele *et al.* (1998). *Phys. Rev. Lett.* **80**, 736–739. Copyright (1998) by the American Physical Society.

3.4. Other polymerization processes

Modifications of C_{60} films have been induced by 3 eV electron irradiation from a scanning tunneling microscopy (STM) tip and by 1500 eV electron irradiation from an electron gun (Zhao *et al.*, 1994). They were interpreted as signatures of polymerization and a growth model was proposed although the nature of the polymerization could not be derived. The f.c.c. structure was restored by annealing above 470 K (Zhao *et al.*, 1994).

Plasma-induced polymerization of films (by radio-frequency Ar-ion plasma) was also reported (Takahashi *et al.*, 1993). The polymerized films were amorphous and several types of inter-fullerene cycloaddition bonding were proposed.

A completely different and remarkable procedure was used to produce C_{60} dimers by solid-state mechanochemical reaction. This was achieved by vigorously vibrating a mixture of C_{60} with potassium cyanide KCN under nitrogen (Wang *et al.*, 1997). The proposed reaction pathway results in the selective formation of dimers. The structure was determined by X-ray analysis of the solution-grown crystals, showing that the cages are linked by four-membered rings *via* 2 + 2 cycloaddition, as in the HPHT and photopolymerized dimers (Wang *et al.*, 1997).

4. Concluding remarks

In this overview, I have concentrated on the orientational properties of the C_{60} monomer and polymers in the bulk state. It is worth mentioning that C_{60} surfaces and films are of considerable theoretical and experimental interest for studying surface ordering and phase transitions in molecular solids. As an example, in the case of the (111) C_{60} surface it was first discovered, using high-resolution electron-energy-loss spectroscopy, that the surface layer orders at 230 K, *i.e.*

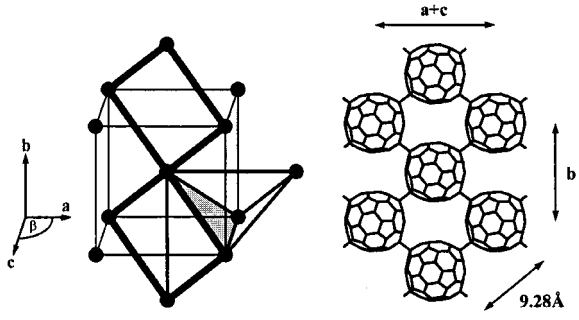

Figure 19
Left: Body-centered monoclinic unit cell of Na_4C_{60}. Filled circles denote fullerene molecules; $(10\bar{1})$ polymer planes are emphasized by heavy lines connecting the molecules. The two types of face-sharing tetrahedra that enclose sodium cations are also shown. Right: Polymer plane of C_{60} showing the correct orientation and approximate distortion of the molecule. Orientational disorder in *I*2/*m* is described by a twofold rotation around **b**. Reprinted with permission from Oszlányi *et al.* (1997). *Phys. Rev. Lett.* **78**, 4438–4441. Copyright (1997) by the American Physical Society.

30 K lower than the bulk (Goldoni *et al.*, 1996). This phenomenon was studied by Monte Carlo simulations (Laforge *et al.*, 2001), which revealed in fact the existence of a two-stage orientational ordering transition with an intermediate partially ordered regime, between 230 and 150 K. At low-temperature, a 2×2 superlattice is stabilized and it consists of ordered molecules whose orientation was imaged by STM (Wang *et al.*, 2001).

The adsorption of C_{60} (or other fullerene) layers on various substrates, metallic or non-metallic, allows one to study the effect of competing C_{60}–C_{60} and C_{60}–substrate interactions. Various commensurate and incommensurate structures have been identified through the analysis of results obtained by LEED, STM and electron spectroscopies (Maxwell *et al.*, 1998; Goldoni *et al.*, 2000; Hsu & Pai, 2003). Interestingly, these C_{60} films can be subsequently doped with alkali metals and studied by angle-resolved photoemission. It was shown, in particular, that the measured Fermi surface and band structure of these doped layers depend on the molecular orientation (Yang *et al.*, 2003).

I have limited this review to a few representative topics that illustrate the important role played by orientational phenomena in the fullerene compounds. Actually, 'orientation' is almost everywhere in this field and many other examples would have been worth describing. To begin with, C_{70} and the higher fullerenes exhibit orientational properties that reflect their less symmetric and non-spherical shape. Concerning doped non-polymeric materials, the superconducting properties of the A_3C_{60} and Na_2AC_{60} compounds are strongly influenced by the orientational state of the molecules (as reviewed by Forró & Mihály, 2001). Another field is that of the many compounds synthesized by fullerene chemistry, where fullerenes are modified, functionalized or combined with other molecules. Here also the orientational degrees of freedom are essential as they determine, for a large part, the properties and phase diagrams [as in C_{60}–biphenyl, where there is a coupling of the C_{60} and biphenyl orientational orderings (Marucci *et al.*, 2002)].

I would like to thank the scientists who have enriched my knowledge on the properties of the fullerene compounds on the occasion of discussions, meetings and conferences. This includes my colleagues at Orsay and in particular Pascale Launois and Sylvain Ravy; the three of us have lived in close and fruitful intimacy with C_{60} for several years. Finally I wish to acknowledge the authors who have authorized publication of material extracted from their articles.

References

Agafonov, V., Davydov, V. A., Kashevarova, L. S., Rakhmanina, A. V., Kahn-Harari, A., Dubois, P., Ceíolin, R. & Szwarc, H. (1997). *Chem. Phys. Lett.* **267**, 193–198.

Andersson, O., Soldatov, A. & Sundqvist, B. (1996). *Phys. Rev. B*, **54**, 3093–3100.

Axe, J. D., Chow, P. C., Moss, S. C. & Wochner, P. (1996). *Physica (Utrecht)*, B**219&220**, 121.

Bendele, G. M., Stephens, P. W., Prassides, K., Vavekis, K., Kordatos, K. & Tanigaki, K. (1998). *Phys. Rev. Lett.* **80**, 736–739.

Bennington, S. M., Kitamura, N., Cain, M. G., Lewis, M. H., Wood, R. A., Fukumi, A. K. & Funakoshi, K. (2000). *J. Phys. Condens. Matter*, **12**, L451–L456.

Blank, V. D., Buga, S. G., Dubitsky, G. A., Serebryanaya, N. R., Popov, M. Yu. & Sundqvist, B. (1998). *Carbon*, **36**, 319–343.

Blank, V. D., Denisov, V. N., Ivlev, A. N., Mavrin, B. N., Serebryanaya, N. R., Dubitsky, G. A., Sulyanov, S. N., Popov, M. Yu., Lvova, N. A., Buga, S. G. & Kremkova, G. N. (1998). *Carbon*, **36**, 1263–1267.

Brazhkin, V. V., Lyapin, A. G. & Popova, S. V. (1996). *Pis'ma Zh. Eksp. Teor. Fiz.* **64**, 755–759. Engl. transl: *JETP Lett.* **64**, 802–807.

Burger, B., Winter, J. & Kuzmany, H. (1996). *Z. Phys.* **101**, 227–233.

Burgos, E., Halac, E. & Bonadeo, H. (1994). *Phys. Rev. B*, **49**, 15544–15549.

Chaplot, S. L. & Pintschovius, L. (1999). *Int. J. Mod. Phys.* **13**, 217–252.

Chaplot, S. L., Pintschovius, L., Haluška, M. & Kuzmany, H. (1995). *Phys. Rev. B*, **51**, 17028–17034.

Chauvet, O., Oszlányi, G., Forró, L., Stephens, P. W., Tegze, M., Faigel, G. & Jánossy, A. (1994). *Phys. Rev. Lett.* **72**, 2721–2724.

Chen, X. & Yamanaka, S. (2002). *Chem. Phys. Lett.* **360**, 501–508.

Chen, X., Yamanaka, S., Sako, K., Inoue, Y. & Yasukawa, M. (2002). *Chem. Phys. Lett.* **356**, 291–297.

Chow, P. C., Jiang, X., Reiter, G., Wochner, P., Moss, S. C., Axe, J. D., Hanson, J. C., McMullan, R. K., Meng, R. L. & Chu, C. W. (1992). *Phys. Rev. Lett.* **69**, 2943–2946.

Copley, J. R. D., David, W. I. F. & Neumann, D. A. (1994). *Neutron News*, **4**, 20–28.

Copley, J. R. D. & Michel, K. H. (1993). *J. Phys. Condens. Matter*, **5**, 4353–4370.

Copley, J. R. D. & Michel, K. H. (1998). *Physica (Utrecht)*, B**241**, 454–455.

Copley, J. R. D., Neumann, D. A., Cappelletti, R. L. & Kamitakahara, W. A. (1992). *J. Phys. Chem. Solids*, **53**, 1353–1371.

Dam Hieu Chi, Iwasa, Y., Takano, T., Watanuki, T., Ohishi, Y. & Yamanaka, S. (2003). *Phys. Rev. B*, **68**, 153402-1–4.

David, W. I. F. & Ibberson, R. M. (1993). *J. Phys. Condens. Matter*, **5**, 7923–7928.

David, W. I. F., Ibberson, R. M., Dennis, T. J. S., Hare, J. P. & Prassides, K. (1992*a*). *Europhys. Lett.* **18**, 219–225.

David, W. I. F., Ibberson, R. M., Dennis, T. J. S., Hare, J. P. & Prassides, K. (1992*b*). *Europhys. Lett.* **18**, 735–736.

David, W. I. F., Ibberson, R. M. & Matsuo, T. (1993). *Proc. R. Soc. London Ser. A*, **442**, 129–146.

Davydov, V. A., Kashevarova, L. S., Rakhmanina, A. V., Agafonov, V. N., Allouchi, H., Ceolin, R., Dzyabchenko, A.V., Senyavin, V. M. & Szwarc, H. (1998). *Phys. Rev. B*, **58**, 14786–14790.

Davydov, V. A., Kashevarova, L. S., Rakhmanina, A. V., Agafonov, V. N., Allouchi, H., Ceolin, R., Dzyabchenko, A. V., Senyavin, V. M., Szwarc, H., Tanaka, T. & Komatsu, K. (1999). *J. Phys. Chem. B*, **103**, 1800–1804.

Dresselhaus, M. S., Dresselhaus, G. & Eklund, P. C. (1996). *Science of Fullerenes and Carbon Nanotubes*. San Diego, CA: Academic Press.

Dzyabchenko, A. V., Agafonov, V. & Davydov, V. A. (1999*a*). *J. Phys. Chem. B*, **103**, 2812–2820.

Dzyabchenko, A. V. Agafonov, V. & Davydov, V. A. (1999*b*). *Crystallogr. Rep.* **44**, 13–17.

Dzyabchenko, A. V. Agafonov, V. & Davydov, V. A. (1999*c*). *Crystallogr. Rep.* **44**, 18–24.

Forró, L. & Mihály, L. (2001). *Rep. Prog. Phys.* **64**, 649–699.

Goldoni, A., Cepek, C. & Modesti, S. (1996). *Phys. Rev. B*, **54**, 2890–2895.

Goldoni, A., Sangaletti, L., Friedmann, S. L., Shen, Z. X., Peloi, M., Parmigiani, F., Comelli, G. & Paolucci, G. (2000). *J. Chem. Phys.* **113**, 8266–8275.

Gránásy, L., Pekker, S. & Forró, L. (1996). *Phys. Rev. B*, **54**, 11849–11852.

Gugenberger, F., Heid, R., Meingast, C., Adelmann, P., Braun, M., Wtihl, H., Haluska, M. & Kuzmany, H. (1992). *Phys. Rev. Lett.* **69**, 3774–3777.

Gunnarsson, O. (1997). *Rev. Mod. Phys.* **69**, 575–606.

Heiney, P. A., Fischer, J. E., McGhie, A. R., Romanow, W. J., Denenstein, A. M., McCauley, J. P. Jr, Smith, A. B. III & Cox, D. E. (1991). *Phys. Rev. Lett.* **66**, 2911–2914.

Hodeau, J. L., Tonnerre, J. M., Bouchet-Fabre, B., Nuñez-Regueiro, M., Capponi, J. J. & Perroux, M. (1994). *Phys. Rev. B*, **50**, 10311–10314.

Hone, J., Fuhrer, M. S., Khazeni, K. & Zettl, A. (1995). *Phys. Rev. B*, **52**, R8700–8702.

Horikawa, T., Suito, K., Kobayashi, M. & Onodera, A. (2001). *Phys. Lett.* A**287**, 143–151.

Hsu, C.-L. & Pai, W. W. (2003). *Phys. Rev. B*, **68**, 245414-1–12.

Huq, A., Stephens, P. W., Bendele, G. M. & Ibberson R. M. (2001). *Chem. Phys. Lett.* **347**, 13–22.

Kosaka, M., Tanigaki, K., Tanaka, T., Atake, T., Lappas, A. & Prassides, K. (1995). *Phys. Rev. B*, **51**, 12018–12021.

Krätschmer, W., Lamb, L. D., Fostiropoulos, K. & Huffman, D. R. (1990). *Nature (London)*, **347**, 354–358.

Kroto, H. W., Heath, J. R., O' Brien, S. C., Curl, R. F. & Smalley, R. E. (1985). *Nature (London)*, **318,** 162–163.

Kuzmany, H., Matus, M., Burger, B. & Winkler, J. (1994). *Adv. Mater.* **6**, 731–745.

Laforge, C., Passerone, D., Harris, A. B., Lambin, P. & Tosatti, E. (2001). *Phys. Rev. Lett.* **87**, 085503-1–4.

Lamoen, D. & Michel, K. H. (1993). *Z. Phys. Teil B*, **92**, 323–330.

Lamoen, D. & Michel, K.H. (1994). *J. Chem. Phys.* **101**, 1435–1443.

Launois, P., Moret, R., Erwin, S. C., Hone, J. & Zettl, A. (1999). *Electronic Properties of Fullerenes. Science and Technology of Molecular Nanostructures. AIP. Conf. Proc.* **486**, 47–51.

Launois, P., Moret, R., Hone, J. & Zettl, A. (1998) *Phys. Rev. Lett.* **81**, 4420–4423.

Launois, P., Ravy, S. & Moret, R. (1995). *Phys Rev. B*, **52**, 5414–5425.

Launois, P., Ravy, S. & Moret, R. (1997*a*). *Phys Rev. B*, **55**, 2651–2665.

Launois, P., Ravy, S. & Moret, R. (1997*b*). *Phys Rev. B*, **56**, 7019–7021.

Launois, P., Ravy, S. & Moret, R. (1999). *Int. J. Mod. Phys.* **13**, 253–281.

Léger, J. M., Haines, J., Davydov, V. A. & Agafonov, V. (2002). *Solid State Commun.* **121**, 241–244.

Lundin, A. & Sundqvist, B. (1996). *Phys. Rev. B*, **53**, 8329–8336.

Margadonna, S., Brown, C. M., Lappas, A., Prassides, K., Tanigaki, K., Knudsen, K. D., Le Bihan, T. & Mezouar, M. (1999). *J. Solid State Chem.* **145**, 471–478.

Marques, L., Hodeau, J. L., Nuñez-Regueiro, M. & Perroux, M. (1996). *Phys. Rev. B*, **54**, R12633–12636.

Marques, L., Mezouar, M., Hodeau, J. L. & Nuñez-Regueiro, M. (2003). *Phys. Rev. B*, **68**, 193408-1–4.

Marques, L., Mezouar, M., Hodeau, J. L., Nuñez-Regueiro, M., Serebryanaya, N. R., Ivdenko, V. A., Blank, V. D. & Dubitsky, G. A. (1999). *Science*, **283**, 1720–1723.

Marucci, A., Launois, P., Moret, R. & Pénicaud, A. (2002). *Eur. Phys. J.* B**26**, 29–34.

Matsuo, T., Suga, H., David, W. I. F., Ibberson, R. M., Bernier, P., Zahab, A., Fabre, C., Rassat, A. & Dworkin, A. (1992). *Solid State Commun.* **83**, 711–715.

Maxwell, A. J., Brühwiler, P. A., Arvanitis, D., Hasselström, J., Johansson, M. K.-J. & Mårsson, N. (1998). *Phys. Rev. B*, **57**, 7312–7326.

Meingast, C. & Gugenberger, F. (1993). *Mod. Phys. Lett B*, **7**, 1703–1724.

Meletov, K. P., Assimopoulos, S., Tsilika, I., Kourouklis, G. A., Arvanitidis, J., Ves, S., Sundqvist, B. & Wågberg, T. (2001). *Chem. Phys. Lett.* **341**, 435–441.

Michel, K. H. & Copley, J. R. D. (1997). *Z. Phys.* B**103**, 369–376.

Michel, K. H., Copley, J. R. D. & Neumann, D. A. (1992). *Phys. Rev. Lett.* **68**, 2929–2932.

Miyake, T. & Saito, S. (2003). *Phys. Rev. B*, **68**, 235402-1–5.

Moret, R. (1993). *Phys. Rev. B*, **48**, 17619–17621.

Moret, R., Launois, P., Persson, P.-A. & Sundqvist, B. (1997). *Europhys. Lett.* **40**, 55–60.

Moret, R., Launois, P. & Ravy S. (1996). *Fullerene Sci. Technol.* **4**, 1287–1298.

Moret, R., Launois, P., Ravy, S., Julier, M. & Godard, J. M. (1997). *Synth. Met.* **86**, 2327–2328.

Moret, R., Launois, P., Wågberg, T. & Sundqvist, B. (2000*a*). *Eur. Phys. J.* B**15**, 253–263.

Moret, R., Launois, P., Wågberg, T. & Sundqvist, B. (2000*b*). *Electronic Properties of Novel Materials/Molecular Nanostructures. AIP Conf. Proc.* **544**, 81–84.

Moret, R., Launois, P., Wågberg, T., Sundqvist, B., Agafonov, V., Davydov, V. A. & Rakhmanina, A. V. (2004) *Eur. Phys. J. B*, **37**, 25–37.

Moret, R., Ravy, S. & Godard, J. M. (1992). *J. Phys. (Paris) I*, **2**, 1699–1704.

Moret, R., Ravy, S. & Godard, J. M. (1993). *J. Phys. (Paris) I*, **3**, 1085.

Moret, R., Wågberg, T. & Sundqvist, B. (2004). *Carbon*. In the press.

Narymbetov, B., Agafonov, V., Davydov, V. A., Kashevarove, L. S., Rakhmanina, A. V., Dzyabchenko, A. V., Kuvalov, V. I. & Céolin, R. (2003). *Chem. Phys. Lett.* **367**, 157–162.

Neumann, D. A., Copley, J. R. D., Kamitakahara, W. A., Rush, J. J., Cappelletti, R. L., Coustel, N., Fischer, J. E., McCauley, J. P., Smith, A. B. III, Creegan, K. M. & Cox, D. M. (1992). *J. Chem. Phys.* **96**, 8631–8633.

Nuñez-Regueiro, M., Marques, L., Hodeau, J.-L., Beíthoux, O. & Perroux, M. (1995). *Phys. Rev. Lett.* **74**, 278–281.

Okada, S. & Oshiyama, A. (2003). *Chem. Phys. Lett.* **380**, 589–594.

Okada, S., Saito, S. & Oshiyama, A. (1999). *Phys. Rev. Lett.* **83**, 1986–1989.

Oszlányi, G., Baumgartner, G., Faigel, G. & Forró, L. (1997). *Phys. Rev. Lett.* **78**, 4438–4441.

Oszlányi, G., Baumgartner, G., Faigel, G., Gránásy, L. & Forró, L. (1998). *Phys. Rev. B*, **58**, 5–7.

Oszlányi, G., Bortel, G., Faigel, G., Gránásy, L., Bendele, G., Stephens, P. W. & Forró, L. (1996). *Phys. Rev. B*, **54**, 11849–11852.

Oszlányi, G., Bortel, G., Faigel, G., Tegze, M., Gránásy, L., Pekker, S., Stephens, P. W., Bendele, G., Dinnebier, R., Mihály, G., Jánossy, A., Chauvet, O. & Forró, L. (1995). *Phys. Rev. B*, **51**, 12228–12232.

Papoular, R. J., Roth, G., Heger, G., Haluska, M. & Kuzmany, H. (1993). *Electronic Properties of Fullerenes. Springer Series in Solid State Sciences*, No. 117, edited by H. Kuzmany, J. Fink, M. Mehring & S. Roth. Berlin: Springer Verlag.

Pekker, S., Jánossy, A., Mihály, L, Chauvet, O., Carrard, M. & Forró, L. (1994). *Science*, **265**, 1077–1078.

Pekker, S., Oszlányi, G. & Faigel, G. (1998). *Chem. Phys. Lett* **282**, 435–441.

Pintschovius, L. (1996). *Rep. Prog. Phys.* **59**, 473–510.

Pintschovius, L., Blaschko, O., Krexner, G. & Pyka, N. (1999). *Phys. Rev. B*, **59**, 11020–11026.

Pintschovius, L., Chaplot, S. L., Roth, G. & Heger, G. (1995). *Phys. Rev. Lett.* **75**, 2843–2846.

Prassides, K., Tanigaki, K. & Iwasa, Y. (1997). *Physica (Utrecht)*, C**282–287**, 307–310.

Rao, A. M., Zhou, P., Wang, K.-A., Hager, G. T., Holden, J. M., Wang, Y., Lee, W.-T., Bi, X.-X., Eklund, P. C., Cornett, D. S., Duncan, M. A. & Amster, I. J. (1993). *Science*, **259**, 955–957.

Ravy, S., Launois, P. & Moret, R. (1996*a*). *Phys Rev. B*, **53**, 10532–10535

Ravy, S., Launois, P. & Moret, R. (1996*b*). *Phys Rev. B*, **54**, 17224.

Rosseinsky, M. J. (1998). *Chem. Mater.* **10**, 2665–2685.

Rouzière, S., Margadonna, S., Prassides, K. & Fitch, A. N. (2000). *Europhys. Lett.* **51**, 314–319.

Ruoff, R. S. & Ruoff, A. L. (1991). *Nature (London)*, **350**, 663–664.

Samara, G. A., Hansen, L. V., Assink, R. A., Morosin, B., Schirber, J. E. & Loy, D. (1993). *Phys. Rev. B*, **47**, 4756–4764.
Savin, S., Harris, A. B. & Yildirim, T. (1997). *Phys Rev. B*, **55**, 14182–14199.
Schiebel, P., Wulf, K., Prandl, W., Heger, G., Papoular, R. & Paulus, W. (1996). *Acta Cryst.* A**52**, 176–188.
Schirber, J. E., Morosin, B., Kwei, G. H., Yildirim, T., Fischer, J. E. & Jorgensen, J. D. (2001). *Physica (Utrecht)*, C**353**, 207–212.
Schranz, W., Fuith, A., Dolinar, P., Warhanek, H., Haluska, M. & Kuzmany, H. (1993). *Phys. Rev. Lett.* **71**, 1561–1564.
Serebryanaya, N. R., Blank, V. D., Ivdenko, V. A. & Chernozatonskii, L. A. (2001). *Solid State Commun.* **118**, 183–187.
Serebryanaya, N. R. & Chernozatonskii, L. A. (2000). *Solid State Commun.* **114**, 537–541.
Simovič, B., Jérome, D., Rachdi, F., Baumgartner, G. & Forró, L. (1999) *Phys. Rev. Lett.* **82**, 2298–2301.
Stephens, P. W., Bortel, G., Fagel, G., Tegze, M., Jánossy, A., Pekker, S., Oszlányi, G. & Forró, L. (1994). *Nature (London)*, **370**, 636–639.
Sundqvist, B. (1999). *Adv. Phys.* **48**, 1–134.
Sundqvist, B. (2001). *Phys. Status Solidi B*, **223**, 469–477.
Takahashi, N., Dock, H., Matsuzawa, N. & Ata, M. (1993). *J. Appl. Phys.* **74**, 5790–5798.
Talyzin, A. V. & Dubrovinsky, L. S. (2003). *Phys. Rev. B*, **68**, 233207-1–4.
Tomaselli, M., Meier, B.H., Riccò, M., Shiroka, T. & Sartori, A. (2001). *Phys. Rev. B*, **63**, 113405-1–4.
Verberck, B., Michel, K. H. & Nikolaev, A. V. (2002). *J. Chem. Phys.* **116**, 10462–10474.
Verberck, B., Nikolaev, A. V. & Michel, K. H. (2002). *Phys. Rev. B*, **66**, 165425-1–14.
Wågberg, T., Jacobsson, P. & Sundqvist, B. (1999). *Phys. Rev. B*, **60**, 4535–4538.
Wågberg, T., Soldatov, A. & Sundqvist, B. (2005). To be published.
Wågberg, T., Stenmark, P. & Sundqvist, B. (2004). *J. Phys. Chem. Solids*, **65**, 317–320.
Wang, G.-W., Komatsu, K., Murata, Y. & Shiro, M. (1997). *Nature (London)*, **387**, 583–586.
Wang, H., Zeng, C., Wang, B., Hou, J. G., Li, Q. & Yang, J. (2001). *Phys. Rev. B*, **63**, 085417-1–5.
Winter, J. & Kuzmany, H. (1992) *Solid State Commun.* **84**, 935–938.
Wulf, K., Schiebel, P., Prandl, W., Paulus, W. & Heger, G. (1999). *J. Phys. Condens. Matter*, **11**, 2493–2501.
Yang, W. L., Brouet, V., Zhou, X. J., Choi, H. J., Louie, S. G., Cohen, M. L., Kellar, S. A., Bogdanov, P. V., Lanzara, A., Goldoni, A., Parmigiani, F., Hussain, Z. & Shen, Z.-X. (2003). *Science*, **300**, 303–307.
Yasukawa, M. & Yamanaka, S. (2001). *Chem. Phys. Lett.* **341**, 467–475.
Zhao, Y. B., Poirier, D. M., Pechman, R. J. & Weaver, J. H. (1994). *Appl. Phys. Lett.* **64**, 577–579.
Zhu, Q., Cox, D. E. & Fischer, J. E. (1995). *Phys. Rev. B*, **51**, 3966–3969.